arXiv:1201.3253v1 [cond-mat.quant-gas] 16 Jan 2012

Probing Atomic Majorana Fermions in Optical Lattices

Christina V. Kraus,[1, 2] Sebastian Diehl,[1, 2] Peter Zoller,[1, 2] and Mikhail A. Baranov[1, 2, 3]
[1] *Institute for Quantum Optics and Quantum Information of the Austrian Academy of Sciences, A-6020 Innsbruck, Austria*
[2] *Institute for Theoretical Physics, University of Innsbruck, A-6020 Innsbruck, Austria*
[3] *RRC “Kurchatov Institute”, Kurchatov Square 1, 123182 Moscow, Russia*

We introduce a one-dimensional system of fermionic atoms in an optical lattice whose phase diagram includes topological states of different symmetry classes. These states can be identified by their zero-energy edge modes which are Majorana fermions. We propose several universal methods of detecting the Majorana edge states, based on their genuine features: zero-energy, localized character of the wave functions, and induced non-local fermionic correlations.

There is at present growing interest in topological phases of matter – fermionic insulators and superconductors with gapped excitation spectrum and nonlocal topological order (TO). TO is characterized by a topological invariant taking discrete values [1–6]. A striking consequence of TO is the existence of robust zero-energy modes localized at defects, edges, and interfaces between different topological phases [7–9]. The number of these states and their properties are directly linked to TO and, therefore, can be viewed as a probe of the topological state providing access to the corresponding phase diagram. A striking example are zero-energy Majorana fermions, as discussed in the context of topological quantum computing [10–12]. Being widely discussed in both high energy and condensed matter theory, the observation of Majorana fermions has so far been elusive, and thus remains an outstanding challenge for both experiment and theory.

Most of the developments and proposals in realizations and studies of topological states of matter in general, and Majorana fermions in particular, have been related to condensed matter systems (see e.g. [13–17]). Many-body systems of cold atoms and molecules, on the other hand, promise not only a clean realization of these phases due to the control available there [18–23], but also a plethora of new measurement techniques [24], as illustrated by the recent achievement of single site addressing and detection in optical lattices [25, 26]. In light of these advances, we study below the signatures of Majorana fermions, and the related measurement of topological phases and phase transitions by available experimental techniques, including time of flight [27] and probe spectroscopy. This complements the analysis of the topological invariant in the bulk as proposed in [28–30]. We illustrate our ideas in the context of two examples. We first propose an atomic “zig-zag Kitaev chain” in an optical lattice (c.f. Fig. 1a)): this provides a model with a rich topological phase diagram, allowing different topological states in two symmetry classes supporting Majorana edge modes, as a test ground for various detection techniques. The presence of TO and the topological phase transitions can be studied by detecting the related Majorana edge states. We discuss several universal methods to detect them via their main features, (i) zero-energy, (ii) localization near the edge and (iii) induced non-local fermionic correlations. Finally, we extend these ideas to the case of an atomic $p_x + ip_y$ superfluid.

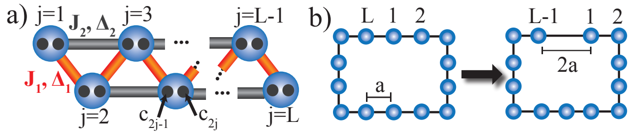

FIG. 1. (Color online) (a) A zig-zag chain of spinless fermonic atoms according to the Hamiltonian H. This geometry allows for an experimental control over the relative strength of NN (red) and NNN couplings (grey). c_{2j-1} and c_{2j} denote Majorana operators on lattice sites $j = 1$ to L (see text). b) Preparation of the initial state of Majorana fermions by adiabatically cutting the closed chain.

Model of a zig-zag Kitaev chain: We consider single-component fermions on a finite chain (one-dimensional (1*d*) lattice) of size L with Hamiltonian $H = H_1 + H_2 + H_\mu$. Here, $H_\mu = -\mu \sum_{j=1}^{L} a_j^\dagger a_j$, and

$$H_\alpha = \sum_{j=1}^{L-\alpha} \left[-J_\alpha a_j^\dagger a_{j+\alpha} + \Delta_\alpha a_j a_{j+\alpha} + h.c. \right],$$

where a_i and $a_i^\dagger$ are fermionic operators ($i = 1, \dots, L$), $J_\alpha \geq 0$ and $\Delta_\alpha = |\Delta_\alpha| e^{i\phi_\alpha}$ are nearest- (NN, $\alpha = 1$) and next-to-nearest-neighbour (NNN, $\alpha = 2$) hopping and pairing amplitudes, respectively, and μ is the chemical potential. H can be viewed as a Hamiltonian of two coupled Kitaev chains [31] (with odd or even sites). In Fig. 1a) we represent the chain as a zig-zag, which leads naturally to a cold atom implementation with optical lattices [22] as the relative strength of NN and NNN amplitudes can be controlled by changing the zig-zag geometry. The pairing terms in H_α are obtained by a Raman induced dissociation of Cooper pairs (or Feshbach molecules) forming an atomic BCS reservoir, with μ a Raman detuning.

The symmetries of H and the corresponding symmetry class [1] depend crucially on the relative phase $\phi = \phi_1 - \phi_2$ of the pairing amplitudes (one of the phases, say, ϕ_2, can be gauged away by redefining the operators

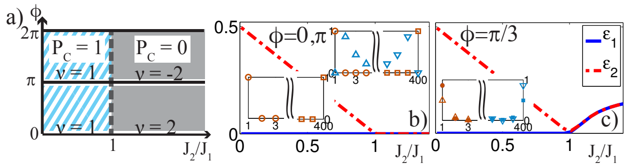

FIG. 2. (Color online) a) Phase diagram corresponding to the Hamiltonian H for $\mu = 0$, $|\Delta_\alpha| = J_\alpha e^{i\phi}$. b) The two lowest eigenvalues $\varepsilon_{1,2}$ of H as a function of the ratio J_2/J_1: If $\phi = 0, \pi \pmod{2\pi}$ (BDI class) there are one or two such modes (b), for all other values of ϕ (D class), there is at most one zero mode (c).

a_j). For $\phi = 0, \pi \pmod{2\pi}$ it is in the class BDI with time-reversal, particle-hole, and chiral symmetries, for all other values of ϕ it is class D with only particle-hole symmetry [38]. Both classes allow topologically nontrivial states characterized by the integer-valued winding number $\nu \in \mathbb{Z}$ in the class BDI and by the Chern parity number $P_C = 0, 1 \in \mathbb{Z}_2$ in the class D. Since we discuss the topological phase diagram of H in full generality elsewhere, we summarize here only the relevant features for our detection schemes. The phase diagram contains states with $\nu = 0, \pm 1, \pm 2$ for the BDI class, and with $P_C = 0, 1$ for the D class. Fig. 2a) summarizes results for the simplest case $\mu = 0$ and $|\Delta_\alpha| = J_\alpha$, where the phase diagram is characterized by the relative phase ϕ and the ratio J_2/J_1. We find that $\nu = P_C = 1$ for $J_1 > J_2$, else one has $P_C = 0$ and $\nu = +2$ or -2 for $\phi = 0$ and π, respectively. Therefore, for both symmetry classes, the point $J_1 = J_2$ corresponds to a topological phase transition, where the bulk excitations become *gapless* [38].

The presence of a nontrivial TO in the bulk leads to zero-energy modes at the interfaces between states with different TO. The number of these states is related to the difference of the corresponding topological invariants [8, 9], which in our case are Majorana fermions. Using the hermitian Majorana representation, where $c_{2j-1} = a_j^\dagger + a_j$ and $c_{2j} = (-i)(a_j^\dagger - a_j)$ obey $\{c_j, c_l\} = 2\delta_{jl}$, the quadratic Hamiltonian reads $H = i\sum_{j,l} A_{jl} c_j c_l$ with real $A = -A^T$. Diagonalizing A for a finite chain we identify the zero-energy modes and associated Majorana edge-mode operator $\gamma_E = \sum_k v_{Ek} c_k$ with (real) coefficients v_{Ek} localized at the interface with some localization length l_{loc}. [To be precise, the energy of these modes $\sim \exp(-L/l_{\text{loc}})$ approaches zero for $L \to \infty$.]

For the BDI class we have in total two such modes for $J_1 > J_2$: $\gamma_L = c_1$ and $\gamma_R = c_{2L}$ for the left and the right edge, respectively, and four modes for $J_1 < J_2$. The two additional zero modes are exponentially decaying inside the bulk (see Fig.2b) and [38]). For the D class there are two zero-energy modes for $J_1 > J_2$, which decay exponentially inside the chain, and no such modes for $J_1 < J_2$ (Fig. 2c)).

The presence of Majorana zero-energy modes leads to a degeneracy of the ground state: The dimension of the zero-energy subspace is $2^{[N_M/2]}$, where N_M is the number of the Majorana modes (which is always even in our case) and $[x]$ is the integer part of x. A state in this subspace generically has correlations between Majorana operators belonging to different edges of the system, resulting in nonlocal fermionic correlations, in contrast to local correlations in the bulk. For the case with only two Majorana modes ($\nu = 1$ or $P_C = 1$), these nonlocal correlations are related to the fermionic parity: $\langle G_\pm | \gamma_L \gamma_R | G_\pm \rangle = \pm i$ for the ground state $|G_\pm\rangle$ with even ($+$) and odd ($-$) number of fermions, in full analogy to Ref. [31]. The number of Majorana zero-energy edge modes is determined by the topological invariant in the bulk, and by detecting them we can access the full topological phase diagram.

Preparation. Before turning to the detection of the Majorana modes, we briefly comment on preparation procedures [22, 33, 34]. The preparation of a unique state is complicated by the fact that these modes are associated with a zero energy subspace that is insensitive to local perturbations. Thus, starting from a thermal state that has generically no long-range correlations, the available local processes cannot create the latter, and we end up in a completely mixed state in the Majorana subspace. This problem can be overcome by starting with a *closed* quantum chain in a fully paired (and, hence, unique) state corresponding to the ground state of a Hamiltonian (see Fig. 1b)). This state has an *even parity* (all particles are paired) and only local correlations between the sites. Making use of local addressing [25, 26] we can ”cut” the chain: We adiabatically empty a part of the chain (with d sites) by locally raising the chemical potential [11]. As a result, we obtain an *open* Kitaev chain in the *even parity* ground state $|G_+\rangle$ with a non-local correlation $\langle G_+ | \gamma_L \gamma_R | G_+ \rangle = i$ across the chain – a unique feature of the presence of Majorana fermions. For the zig-zag we start with two decoupled subchains (with even and odd number of sites) corresponding to $\Delta_1 = J_1 = 0$ and perform the ”cut”. This leads to two decoupled chains with even parity supporting four Majorana modes. This condition is preserved if we turn on the couplings J_1 and Δ_1 between the subchains until we reach the point of the phase transition. Then, we end up in a state of even parity for the whole chain supporting two Majorana modes [38]. Note that the cutting procedure avoids the need to establish the edge-edge correlations via a sequential process, which takes polynomial time due to the Lieb-Robinson bound [35, 36].

Time-of-Flight (TOF) imaging. Non-local correlations can be detected in TOF imaging, as illustrated in Fig. 3a). We consider atoms of mass m released at time $t = 0$ from lattice sites $R_j = ja$ with lattice spacing a. At time $t \gg ma^2/\hbar$ (far field approximation) the atomic density distribution at the detector is given by $\langle n(x) \rangle \sim \sum_{j,j'} e^{2ix(R_j - R_{j'})m/(\hbar t)} \langle a_j^\dagger a_{j'} \rangle$ revealing the

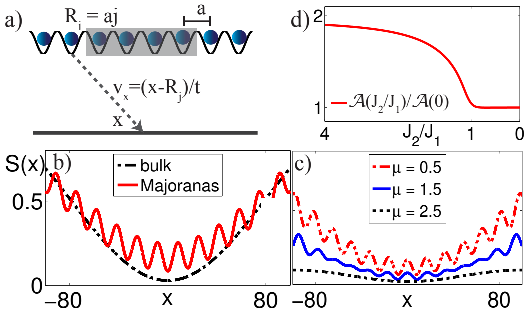

FIG. 3. (Color online) a) Principle of TOF. The signal can be enhanced by excluding the bulk (grey shade). b) TOF for the ideal Kitaev chain: The presence of the Majorana modes (solid) leads to oscillations of the signal $S(x)$ (see main text) which are absent in the bulk (dashed), and vanish if we approach the transition point at $\mu = 2$, see c). d) The amplitude of $S(x)$ allows to determine the number of Majorana modes (see main text).

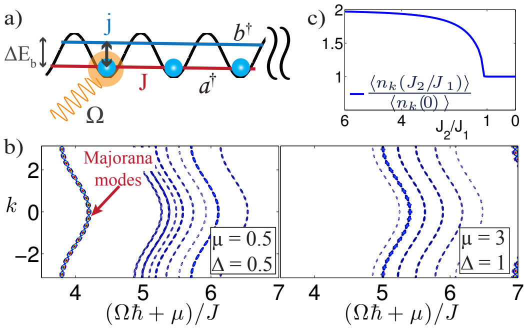

FIG. 4. (Color online) a) Spectroscopic detection of Majorana modes in a two-band lattice (see text). b) The momentum distribution of atoms in the upper band reveals the presence (left) or absence (right) of Majorana modes (see text). c) From the strength of the signal $\langle n_k\rangle$ at resonance (here: $k = \pi/2$) we can deduce the number of Majorana modes.

initial correlations of atoms in the lattice. Therefore, the long-range Majorana correlations $R_j - R_{j'} \approx L_M$ (distance between the edge modes) will result in rapid oscillations of $\langle n(x)\rangle$ as compared to slow oscillations originating from short-range bulk correlations ($R_j - R_{j'} \approx a$). The contrast of the Majorana signal can be enhanced by local addressing: we shade all but N_b sites adjacent to each of the two edges ($N_b = 2$ in Fig. 3a)), thus measuring $\langle n(x)\rangle = 2N_b S(x)$, where we have normalized by the number of sites contributing to the signal, $2N_b$.

For $J_\alpha = \Delta_\alpha$, $J_2 = \mu = 0$ (ideal Kitaev chain), we find

$$\langle n(x)\rangle_+ \sim \mathcal{N}_{bulk}(x) + m(d)\mathcal{N}_{edge}(x),$$

where $\mathcal{N}_{bulk}(x) = 2N_b \sin^2(\frac{mxa}{\hbar t}) + \cos(\frac{mxa}{\hbar t})$ stems from the atoms in the bulk only and the two edge sites separated by $L_M = ad$ give rise to $\mathcal{N}_{edge}(x) = \cos(\frac{mxa}{\hbar t}d)/2$ multiplied by the Majorana correlation $m(d) = -i\langle\gamma_L\gamma_R\rangle$ [38]. Therefore, the second rapidly oscillating term provides information on the presence of the long-range Majorana correlations related to the occupation/purity of the Majorana subspace. If the initial state of the chain is prepared as described above, then $m(d) = -i\langle G_+|\,\gamma_L\gamma_R\,|G_+\rangle = 1$, and the amplitude of this terms reaches its maximum. The results of the calculations for the ideal chain are shown in Fig. 3b): The presence of the Majorana modes leads to oscillations that are absent in the bulk. By ramping the chemical potential, we can detect the location of the phase transition, since the oscillations disappear when crossing the transition point at $\mu = 2$ (see Fig. 3c)). Further, from the amplitude $\mathcal{A}$ of the signal $S(x)$ we can deduce the number of Majorana modes, as depicted in Fig. 3d): The amplitude for four zero modes ($J_2 > J_1$) drops by a factor of two upon reaching the transition point $J_2 = J_1$.

Spectroscopy. The combination of a spectroscopic setup with TOF allows to measure not only the energy of the Majorana states but also their wave functions. Consider a 1d lattice with two bands (modes a_j (b_j) in the upper (lower) band) separated by an energy difference ΔE_b. In the lower band we realize the Hamiltonian H, while the fermions can hop freely with the hopping amplitude j in the upper band. The full Hamiltonian reads $H_0 = H + H_{up}$, where $H_{up} = j\sum_{l=1}^{L}(b_l^\dagger b_{l+1} + h.c.) + \Delta E_b \sum_{l=1}^{L} b_l^\dagger b_l$. We then couple upper and lower bands on the *first* and the *last* sites of an open chain via a time-dependent perturbation $V(t) = V_0(b_1^\dagger a_1 + b_L^\dagger a_L)e^{-i\Omega t} + h.c.$ (see Fig. 4a) and measure the momentum distribution in the upper band as a function of the frequency Ω, e.g., via TOF imaging. Assuming an ideal Kitaev chain in the lower band, the upper band momentum distribution is [38]

$$\begin{aligned}&\langle n_k(t,\Omega)\rangle = V_0^2 M^{-1}(n_0 + n_1), \qquad (1)\\ &n_0 = A_0 f_t(\varepsilon_k - \Omega\hbar), \qquad n_1 = f_t(\varepsilon_k + 2J - \Omega\hbar),\end{aligned}$$

where we have introduced the notation $A_0 = (m_+(d) - m_-(d))\sin^2\frac{k}{2}(L-1) + \lambda_-$ and $f_t(x) = 4\sin^2(xt/2\hbar)/x^2$. Further, $\varepsilon_k = \Delta E_b + 2j\cos k$ is the dispersion in the upper band and $m_\pm(d)$ denote the initial occupation of the even/odd parity subspace in the lower band. The contribution n_0 corresponds to a parity flip in the lower band (no energy cost) and the creation of an excitation in the upper band (energy ε_k). Thus, the absorption peak at $\hbar\Omega = \varepsilon_k$ in n_0 indicates the ground state degeneracy. The edge-edge Majorana correlation length is encoded in the oscillation period. In contrast, the term n_1 results from creation of excitations in both upper (energy ε_k) and lower (energy $2J$) band. The corresponding absorption peak is located at $\hbar\Omega = 2J + \varepsilon_k$, providing the direct measurement of the pairing energy gap ($2J$ here) from the distance of two peaks. Thus, the topologically non-trivial phase leads to a clear signal at $\Omega\hbar = 2J + \mu$ (for $\mu \neq 0$ one has to replace $\hbar\Omega \to \hbar\Omega - \mu$, cf. Fig. 4b)).

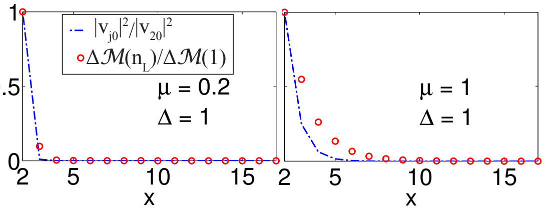

FIG. 5. (Color online) Measurement of the localization length of the Majorana mode via spectroscopy (see main text).

Note that this setup allows to detect the presence of the zero energy Majorana subspace independently of its purity. Further, the number of Majorana modes is encoded in the strength of the resonance signal for a fixed momentum k. In Fig. 4c) we present the results for the Hamiltonian H with $J_\alpha = |\Delta_\alpha|$, $\phi = 0$, where the perturbation is on sites $1, 2, L-1$ and L. Starting from a state with four Majorana modes, we reduce the ratio J_2/J_1. At the transition point, the amplitude of the resonance signal $\langle n_{k=\pi/2}\rangle$ drops to half its magnitude indicating the disappearance of two of the Majorana modes.

With a slight modification of the above setup one can also infer information about the *localization length* of the Majorana zero modes. Namely, we apply the perturbation to the first n_L sites: $V^{(n_L)}(t) = V_0 \sum_{j=1}^{n_L} a_j^\dagger b_j e^{i\Omega t} + h.c.$. The corresponding momentum distribution in the upper band is now

$$\langle n_k(\Omega,t)\rangle = \frac{V_0^2}{M}\sum_{\nu=0}^{L-1} f_t(E_\nu+\epsilon_k-\Omega\hbar)\left|\sum_{j=1}^{n_L} e^{ikj}v_{j\nu}\right|^2, \quad (2)$$

where v_{jl} are the coefficients of the Bogoliubov transformation to the quasiparticle operators $\tilde{a}_\nu$ (ν labels the quasiparticle modes with energies E_ν) in the lower band, $a_i = \sum_j (u_{i\nu}\tilde{a}_\nu - v_{i\nu}^*\tilde{a}_\nu^\dagger)$, which diagonalizes H. Let us now consider $k = 0$ and the external frequency being in resonance with the lowest energy ($\nu = 0$ Majorana) level, $\Omega = \Omega_r = \Delta E_b + \epsilon_{k=0}$. In this case, only the Majorana mode is excited in the lower band, and one has $\langle n_{k=0}(\Omega_r,t)\rangle \sim \left|\sum_{j=1}^{n_L} v_{j0}\right|^2 \equiv \mathcal{M}(n_L)$. The *localized character* of the Majorana mode can now be established by looking at the dependence of $\langle n_{k=0}(\Omega_r,t)\rangle$ on the number of sites n_L affected by the perturbation. To be more specific, the absolute change of $\mathcal{M}(n_L)$ when n_L is increased by one, $\Delta\mathcal{M}(n_L) = |\mathcal{M}(n_L+1) - \mathcal{M}(n_L)|$, is expected to be $\Delta\mathcal{M}(n_L > 1) = 0$ for the ideal Kitaev chain and $\Delta\mathcal{M}(n_L) \sim \exp(-n_L/l_{\rm loc})$ for a generic one. This is reflected in a comparison of the normalized quantity $\Delta\mathcal{M}(n_L)/\Delta\mathcal{M}(1)$ (red circles) with the normalized wave function of the Majorana mode, $|v_{j0}|^2/|v_{20}|^2$ (dashed) as shown in Fig. 5.

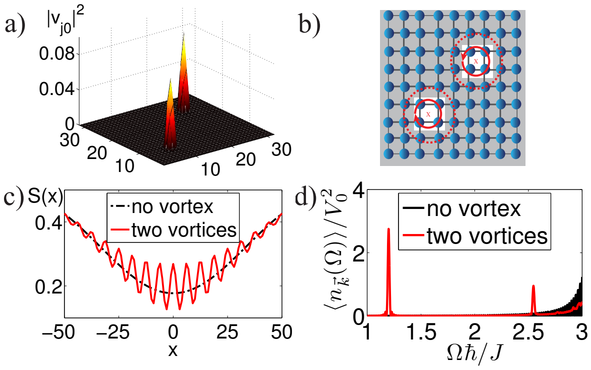

FIG. 6. (Color online) a) Spatial distribution of the Majorana modes in the vicinity of two vortices imprinted on a $p_x + ip_y$-superfluid for $\mu = 2J$ on a 32×32 lattice. b) A shade (grey) is introduced to enhance the signal contrast for the TOF (c) and spectroscopic (d) detections ($\Delta E_B = J, j = 0.1J$).

Probing in 2d. To illustrate the universality of the proposed methods, we apply them to a $2d$ p_x+ip_y superfluid [32, 37] with Hamiltonian $H_S = H_{hopp} + H_{pair} + H_\mu$, with a NN hopping H_{hopp}, a pairing term $H_{pair} = \sum_{\mathbf{x},\mathbf{y}} \Delta_{\mathbf{x},\mathbf{y}} a_{\mathbf{x}}^\dagger a_{\mathbf{y}}^\dagger + h.c.$ where $\Delta_{\mathbf{x},\mathbf{y}} = \Delta_{\mathbf{x}}(\delta_{\mathbf{y},\mathbf{x}+\mathbf{e}_1} + i\delta_{\mathbf{y},\mathbf{x}+\mathbf{e}_2})$, and $H_\mu = -\mu\sum_{\mathbf{x}} a_{\mathbf{x}}^\dagger a_{\mathbf{x}}$. The fermionic operators $a_{\mathbf{x}}$ are defined on a $2d$ (square) lattice and the vectors $\mathbf{e}_{1,2}$ are two independent elementary lattice translations. We introduce two vortices (each with vorticity 1) via a position dependent order parameter $\Delta_{\mathbf{x}} = |\Delta|e^{i\phi(x)}$, which can be written onto the superfluid by phase imprinting in the Raman process [24].

For $|\mu| \ll 4J$ we have a topological ground state supporting two Majorana modes located in the vicinity of the two vortices (cf. Fig. 6 a)). The comparison of the TOF signal with and without vortices (Fig. 6c)) shows that the presence of the Majorana modes leads to an oscillatory behavior of the density $\langle n(x)\rangle$ at the detector. Again, the contrast of the signal is enhanced by shading all but a small region near the vortices (Fig. 6b)). To detect the Majorana modes in the spectroscopic setup, we apply an external perturbation $V(t) = V_0 \sum_{\mathbf{x}\in\Lambda} a_{\mathbf{x}} b_{\mathbf{x}}^\dagger e^{-i\Omega t} + h.c.$, where Λ includes the lattice sites inside a $w \times w$ small regions around the vortices (here: $w = 3$). The resulting momentum distribution in the upper band $\langle n_{k_x,k_y}\rangle$ for $k_{x,y} = \frac{\pi}{32}$ is depicted in Fig. 6d). The presence of the Majorana modes leads to a clear signal at $\Omega\hbar/J = \varepsilon_{\frac{\pi}{32},\frac{\pi}{32}}/J \approx 1.19$ that is absent in a vortex-free setting.

In summary, we have analyzed various scenarios creating topological states of matter with cold atoms, and their reliable detection via time of flight and probe spectroscopy of zero energy Majorana edge modes.

We thank E. Rico for helpful discussions. We acknowledge support by the Austrian Science Fund (FWF) through SFB FOQUS and the START grant Y 581-N16 (S. D.), the European Commission (AQUTE, NAME-QUAM), the Institut fuer Quanteninformation GmbH and the DARPA OLE program.

---

[1] S. Ryu, A. P. Schnyder, A. Furusaki, and A. W. W. Ludwig, New Journal of Physics, **12**(6), 065010 (2010).
[2] A. P. Schnyder, S. Ryu, A. Furusaki, and A. W. W. Ludwig, Phys. Rev. B, **78**, 195125 (2008).
[3] A.Y. Kitaev, AIP Conf. Proc., **1134**, 22 (2008).
[4] X.-L. Qi, T. L. Hughes, and S.-C. Zhang, Phys. Rev. B, **78**, 195424, (2008).
[5] M. R. Zirnbauerm J. Math. Phys., **37**,4986, (1996).
[6] A. Altland and Martin R. Zirnbauer, Phys. Rev. B, **55**, 1142 (1997).
[7] J. C. Y. Teo and C. L. Kane, Phys. Rev. B, **82**, 115120 (2010).
[8] V. Gurarie, Phys. Rev. B, **83**, 085426 (2011).
[9] A. M. Essin and V. Gurarie, Phys. Rev. B, **84**, 125132 (2011).
[10] Jay D. Sau, Roman M. Lutchyn, S. Tewari, and S. Das Sarma, Phys. Rev. Lett., **104**, 040502 (2010).
[11] J. Alicea, Y. Oreg, G. Refael, F. von Oppen, and M. P. A. Fisher, Nature Physics, **7**, 412 (2011).
[12] S. Tewari, S. Das Sarma, C. Nayak, C. Zhang, and P. Zoller, Phys. Rev. Lett., **98**, 010506 (2007).
[13] L. Fu and C. L. Kane, Phys. Rev. Lett., **102**, 216403 (2009).
[14] L. Fu, Phys. Rev. Lett., **104**, 056402 (2010).
[15] J. D. Sau, S. Tewari, R. M. Lutchyn, T. D. Stanescu, and S. Das Sarma, Phys. Rev. B, **82**, 214509 (2010).
[16] A. R. Akhmerov, J. Nilsson, and C. W. J. Beenakker, Phys. Rev. Lett., **102**, 216404 (2009).
[17] T. D. Stanescu, R. M. Lutchyn, and S. Das Sarma, Phys. Rev. B, **84**, 144522 (2011).
[18] N. Goldman, I. Satija, P. Nikolic, A. Bermudez, M. A. Martin-Delgado, M. Lewenstein, and I. B. Spielman, Phys. Rev. Lett., **105**, 255302 (2010).
[19] J. Levinsen, N. R. Cooper, and G. V. Shlyapnikov, Phys. Rev. A, **84**, 013603 (2011).
[20] T. D. Stanescu, V. Galitski, and S. Das Sarma, Phys. Rev. A, **82**, 013608 (2010).
[21] K. Sun, Z. Gu, H. Katsura, and S. Das Sarma, Phys. Rev. Lett., **106**, 236803 (2011).
[22] L. Jiang, T. Kitagawa, J. Alicea, A. R. Akhmerov, D. Pekker, G. Refael, J. I. Cirac, E. Demler, M. D. Lukin, and P. Zoller, Phys. Rev. Lett., **106**, 220402 (2011).
[23] S. Diehl, E. Rico, M. A. Baranov, and P. Zoller, Nat. Phys., **7**, 971 (2011).
[24] Detection methods for Majorana fermions in the condensed matter systems have been proposed by Yaacov E. Kraus, Assa Auerbach, H. A. Fertig, and S. H. Simon, Phys. Rev. B, **79**, 134515 (2009) and E. Grosfeld, N. R. Cooper, A. Stern, and R. Ilan, Phys. Rev. B, **76**, 104516 (2007).
[25] C. Weitenberg, M. Endres, J. F. Sherson, M. Cheneau, P. Schauß, T. Fukuhara, I. Bloch, and S. Kuhr, Nature (London), **471**, 319 (2011).
[26] J. Simon, W. S. Bakr, R. Ma, M. E. Tai, P. M. Preiss, and M. Greiner, Nature (London),**472**, 307 (2011).
[27] I. Bloch, J. Dalibard, and W. Zwerger, Rev. Mod. Phys., **80**, 885 (2008).
[28] E. Zhao, N. Bray-Ali, C. J. Williams, I. B. Spielman, and I. I. Satija, Phys. Rev. A, **84**, 063629 (2011).
[29] E. Alba, X. Fernandez-Gonzalvo, J. Mur-Petit, J. K. Pachos, and J. J. Garcia-Ripoll, Phys. Rev. Lett., **107**, 235301 (2011).
[30] G. Juzeliūnas and I. Spielman, Physics, **4**, 99 (2011).
[31] A. Y. Kitaev, Physics-Uspekhi, **44(10S)**, 131, (2001).
[32] D. A. Ivanov, Phys. Rev. Lett., **86**, 268 (2001).
[33] W. Ketterle and M. W. Zwierlein, Nuovo Cimento Rivista Serie, **31**, 247 (2008).
[34] A. J. Leggett, Quantum Liquids: Bose Condensation and Cooper Pairing in Condensed-Matter Systems. Oxford University Press, USA, 2006.
[35] S. Bravyi, M. B. Hastings, F. Verstraete, Phys. Rev. Lett. **97**, 050401 (2006).
[36] J. Eisert, T. J. Osborne, Phys. Rev. Lett. **97**, 150404 (2006).
[37] N. Read and D. Green, Phys. Rev. B, **61**, 10267 (2000).
[38] See Supplementary Material

SUPPLEMENTARY MATERIAL

Symmetries and phase diagram of the model

Following the general tenfold classification scheme [1, 3], the topological class to which a given Hamiltonian belongs to, is determined by the invariance properties of the Hamiltonian under time-reversal, particle-hole (or charge conjugation), and chiral (or sublattice) symmetry. This class specifies then, whether the states with a nontrivial topological order could exist and provides the corresponding topological invariant to distinguish them.

For a translationally invariant $1d$ spinless Bogoliubov-de Gennes lattice Hamiltonian in the quasimomentum basis

$$H = \sum_{k \in \mathrm{BZ}} \Psi_k^\dagger \mathcal{H}_k \Psi_k,$$

where

$$\mathcal{H}_k = \begin{pmatrix} \xi_k & \Delta_k \\ \Delta_k^* & -\xi_k \end{pmatrix}, \quad \Psi_k = \begin{pmatrix} a_k \\ a_{-k}^\dagger \end{pmatrix},$$

with $a_k = L^{-1/2} \sum_k e^{ikj} a_j$, the invariances are equivalent to the following conditions:

$$U_T^\dagger \mathcal{H}_{-k}^* U_T = \mathcal{H}_k,$$

for the time-reversal,

$$U_C^\dagger \mathcal{H}_{-k}^* U_C = -\mathcal{H}_k,$$

for the particle-hole, and

$$\Sigma^\dagger \mathcal{H}_k \Sigma = -\mathcal{H}_k,$$

for the chiral symmetries, respectively, where U_T, U_C, and Σ are unitary matrices satisfying $U_T U_T^* = \pm 1$, $U_C U_C^* = \pm 1$, and $\Sigma^2 = 1$.

For the Hamiltonian H from the main text one has $\xi_k = -(J_1 \cos k + J_2 \cos 2k) - \mu/2$ and $\Delta_k = -i(\Delta_1 \sin k + \Delta_2 \sin 2k)$, such that the matrix $\mathcal{H}_k$ is

$$\mathcal{H}_k = \vec{h}_k \cdot \vec{\sigma},$$

where $\vec{\sigma} = \{\sigma_x, \sigma_y, \sigma_z\}$ is the vector of Pauli matrices and $\vec{h}_k^T = [\mathrm{Im}(\Delta_k), \mathrm{Re}(\Delta_k), \xi_k]$. The excitation energies are $E_k = 2\left|\vec{h}_k\right| = 2\sqrt{\xi_k^2 + |\Delta_k|^2}$.

For generic $\Delta_1 = |\Delta_1| e^{i\phi_1}$ and $\Delta_2 = |\Delta_2| e^{i\phi_2}$, only the particle-hole symmetry condition is fulfilled with $U_C = \sigma_x$ (as it should be for a general Bogoliubov-de Gennes Hamiltonian), and, therefore, the Hamiltonian H belongs to the class D. For $\phi \equiv \phi_1 - \phi_2 = 0$ or π $(\mathrm{mod}\, 2\pi)$, that is $\Delta_k = -ie^{i\phi_2}(\varepsilon |\Delta_1| \sin k + |\Delta_2| \sin 2k)$ with $\varepsilon = \exp(i\phi) = \pm 1$, the conditions for the time-reversal and chiral symmetries are also satisfied with $U_T = \mathrm{diag}(e^{-i\phi_2}, e^{i\phi_2})$ and $\Sigma = \sigma_x U_T$, and the Hamiltonian H belongs to the chiral BDI class. Note that the phase ϕ_2 can be gauged away by $a_k \to e^{-i\phi_2/2} a_k$ such that $\mathrm{Im}(\Delta_k) = 0$ and the vector $\vec{h}_k$ belongs to the yz-plane for all k. Geometrically speaking, for the BDI class the vectors $\vec{h}_k$ for all k are in the same plane, which is the yz-plane for $\phi_2 = 0$.

For the chiral BDI class in $1d$, different topological states are classified by the integer valued winding number $\nu \in \mathbb{Z}$ defined in the following way (see, for example, [7]): By gauging away the phase ϕ_2 and using a unitary transformation $U = \exp(i\pi\sigma_y/4)$, the Hamiltonian can be transformed into a canonical form

$$\mathcal{H}_k = \begin{pmatrix} 0 & q_k \\ q_k^* & 0 \end{pmatrix} = |q_k| \begin{pmatrix} 0 & e^{i\varphi_{q_k}} \\ e^{-i\varphi_{q_k}} & 0 \end{pmatrix},$$

with $q_k = \xi_k + \Delta_k$ and φ_{q_k} being the phase of q_k. Then

$$\nu = \frac{1}{2\pi} \int_{-\pi}^{\pi} dk \frac{d\varphi_{q_k}}{dk} = \varphi_{q_{k=2\pi}} - \varphi_{q_{k=0}} \in \mathbb{Z}.$$

Alternatively, the winding number can be defined using the unit vector $\vec{n}_k = \vec{h}_k / \left|\vec{h}_k\right|$ in the yz-plane (ϕ_2 is gauged away)

$$\nu = \frac{1}{2\pi} \int_{-\pi}^{\pi} \hat{e}_x \cdot (\vec{n}_k \times \partial_k \vec{n}_k) dk \in \mathbb{Z},$$

as number of times the vector $\vec{n}_k$ wraps around the unit circle when k goes around the Brioullin zone (here $\hat{e}_x$ is the unit vector along the x-axis). Note that as long as $\left|\vec{h}_k\right| \neq 0$ (or, equivalently, $|q_k| \neq 0$), which corresponds to the gapped spectrum of the Hamiltonian, the winding number is well-defined and, therefore, can change its value only when the gap closes. This gap-closing condition is the necessary one for the topological phase transition.

For $|\Delta_\alpha| = J_\alpha$ and $\mu = 0$, the gap closing condition corresponds to $J_1 = J_2$, and straightforward calculations give $\nu_{\phi=0} = -\frac{1}{2}\left[3 - \mathrm{sign}\left(\frac{J_1 - J_2}{J_1 + J_2}\right)\right]$ and $\nu_{\phi=\pi} = \frac{1}{2}\left[3\mathrm{sign}\left(\frac{J_1 - J_2}{J_1 + J_2}\right) - 1\right]$. For $J_1 = J_2$ we indeed have a topological phase transition between two different states. For a finite chain, the winding number manifests itself in the number of zero-energy modes localized near the chain edges, see Figs. 7 a) and 7 b). When one approaches the topological phase transition point, say, from the side $J_2 > J_1$, two out of four zero-energy modes start to proliferate inside the bulk of the chain and become gapped on the other side of the transition; see Fig. 7 c).

The topological phase diagram in this chiral class for the case $|\Delta_1| \neq J_1$, but still $\Delta_2 = J_2$ and $\mu = 0$, is shown in Fig. 8. In this case $\vec{h}_k = (0, \Delta_1 \sin k + J_2 \sin 2k, J_1 \cos k + J_2 \cos 2k)$, where we assume $\phi_2 = 0$, and, hence, real Δ_1. The boundaries between different topological phases results from the condition $\left|\vec{h}_k\right| = 0$.

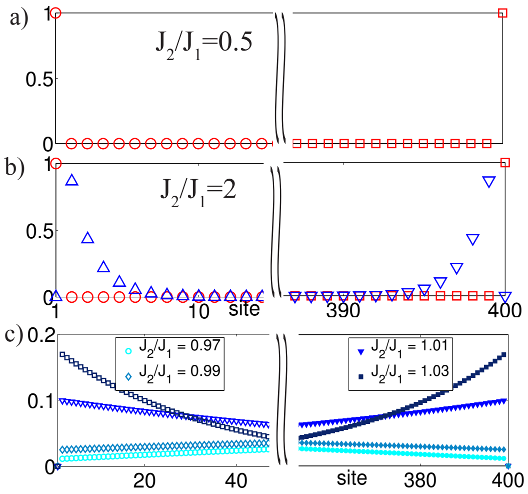

FIG. 7. Spatial distribution of the zero energy modes of H for $J_\alpha = |\Delta_\alpha|$ and $\phi = 0$. a) If $J_2 < J_1$ we have two zero energy modes that are located at the boundary. b) If $J_2 > J_1$, two additional zero energy modes with an exponential decay appear. c) These modes extend more and more over the lattice when we approach the transition point $J_2 = J_1$.

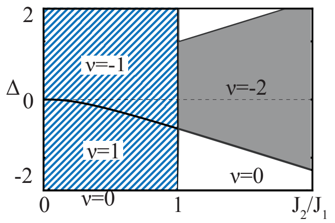

FIG. 8. Topological phase diagram in the chiral class for the case $|\Delta_1| \neq J_1$ but still $\Delta_2 = J_2$ and $\mu = 0$. We see that we can obtain regions with $\nu = 0$ (white), 1 (striped) and 2 (grey).

For the D class [when $\phi \neq 0, \pi (\mathrm{mod}\, 2\pi)$], there are only two different classes of the topological states characterized by the Chern parity number $P_C \in \mathbb{Z}_2$. To define this topological invariant [4], one has to extend the Hamiltonian $\mathcal{H}_k$ and thus $\vec{h}_k$ from a one-dimensional Brillouin zone $k \in [-\pi, \pi] \sim S^1$ (topologically equivalent to the circle S^1) to a two-dimensional ($2d$) Brillouin zone $k, t \in [-\pi, \pi] \sim S^1 \times S^1 = T^2$ (topologically equivalent to a two-dimensional torus T^2), $\mathcal{H}_k \to \mathcal{H}_{k,t} = \vec{h}_{k,t} \cdot \vec{\sigma}$, such that the resulting Hamiltonian is gapped and belongs to the D class in $2d$: $\sigma_x \mathcal{H}^*_{-k,-t} \sigma_x = -\mathcal{H}_{k,t}$. The unit vector $\vec{n}_{k,t} = \vec{h}_{k,t}/|\vec{h}_{k,t}|$ maps then the $2d$ Brillouin zone T^2 into a $2d$ sphere S^2. Different topological classes of such mappings are distinguished by the integer-valued Chern number

$$C = \int_{-\pi}^{\pi} \frac{dk dt}{4\pi} \vec{n}_{k,t} \cdot (\partial_k \vec{n}_{k,t} \times \partial_t \vec{n}_{k,t}) \in \mathbb{Z}.$$

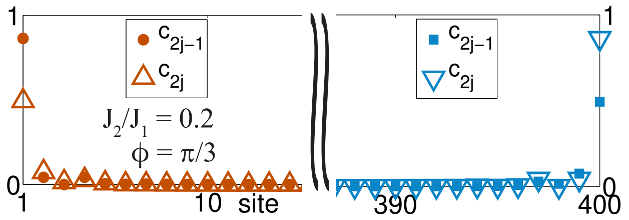

FIG. 9. Spatial distribution of the zero modes for $\phi = \pi/3$ and $J_2/J_1 = 0.2$. There are two zero modes (left and right) which have are linear combinations of only even or only odd Majorana operators living on a site j.

It turns out [4], that the parity P_C of C does not depend on the chosen extension of the Hamiltonian, and, therefore, provides the topological invariant for $1d$ Hamiltonians in the D class. (We set $P_C = 1$ for odd C and $P_C = 0$ for even C. Topologically nontrivial states correspond to $P_C = 1$.)

The extension can be constructed using a hermitian matrix $\bar{\mathfrak{h}}(k,t) = \sum_i \mathfrak{h}_i(k,t)\sigma_i$, which has a gapped spectrum and depends on two parameters $k \in [-\pi, \pi]$ and $t \in [0, \pi]$ such that $\bar{\mathfrak{h}}(k, 0) = \mathcal{H}_k$ and $\bar{\mathfrak{h}}(k, \pi) = |\vec{h}_k|\sigma_z$. Note that $\bar{\mathfrak{h}}(k,t)$ interpolates between the initial Hamiltonian $\mathcal{H}_k$ and the "trivial" one $|\vec{h}_k|\sigma_z$, both from the D class (for $t \neq 0$ or π, $\bar{\mathfrak{h}}(k,t)$ does not necessarily belong to the D class in $1d$). Such a matrix always exists because it belongs to the A class of general hermitian matrices (with no symmetries) with a gapped spectrum that is topologically trivial. Then the matrix

$$\mathcal{H}_{k,t} = \begin{cases} \bar{\mathfrak{h}}(k, \pi + t), & \text{for } t \in [-\pi, 0] \\ -\sigma_1 \bar{\mathfrak{h}}^T(-k, \pi - t)\sigma_1 & \text{for } t \in [0, \pi] \end{cases}$$

is in the D class and provides the desired extension. The interpolation $\bar{\mathfrak{h}}(k,t)$ can be obtained, for example, in the following way: $\mathfrak{h}_i(k,t)$ for $t \in [0, \pi/2]$ corresponds to a rotation of $\vec{h}_k = \mathfrak{h}_i(k, 0)$ to the y-axes, such that $\mathfrak{h}_i(k, \pi/2)$ is parallel to the y-axes for all k, and then $\bar{\mathfrak{h}}(k,t)$ for $t \in [\pi/2, \pi]$ describes the rotation of $\mathfrak{h}_i(k, \pi/2)$ to the z-axis.

Following this strategy for the case $|\Delta_\alpha| = J_\alpha$ with $\mu = 0$ we find $C = 0$ for $J_2 > J_1$ and $C = \mathrm{sign}(\sin\phi)$ for $J_1 > J_2$, where $\phi = \phi_1 - \phi_2$. The point $J_1 = J_2$ corresponds to the topological phase transition, at which the gap vanishes, see Fig.2c).

Preparation of Majorana fermions in 1d

We present here some details on preparation of a unique Majorana fermion state in an open chain. The idea can be illustrated on ideal Kitaev chain ($\Delta_2 = J_2 = 0$ and $\Delta_1 = J_1$). Starting from the ground state of

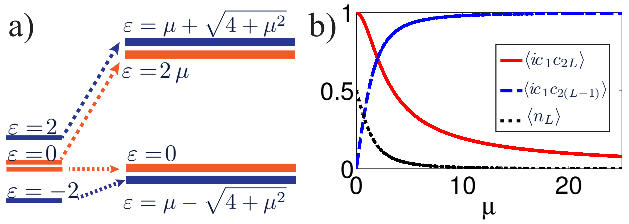

FIG. 10. a)Evolution of energy spectrum of the Hamiltonian $H(\mu) = H_K + \mu(t)a_L^\dagger a_L|_{j=1,L}$ for an adiabatic ramp of μ. b) Evolution of the occupation and Majorana correlation functions during the adiabatic ramp.

a closed chain, we cut it adiabatically by ramping the chemical potential on the site L,

$$H(\mu) = H + \mu(t)a_L^\dagger a_L.$$

This process affects only the four Majorana modes $c_{2L-2}, c_{2L-1}, c_{2L}, c_1$, and the corresponding instantaneous eigenvalues are 0 and 2μ for the odd parity sector, and $\mu \pm \sqrt{4+\mu^2}$ for the even one, such that there are two degenerate ground states of the Kitaev chain for $\mu \to \infty$. Because a superposition of fermionic states with different parity is forbidden by superselection rules, the corresponding eigenstates never mix during the adiabatic ramp (cf. Fig. 10a)), and, hence, the final state of the open chain has even parity. In Fig. 10b) we depict the evolution of the Majorana correlation functions between nearest- ($\langle ic_1c_{2L}\rangle$, solid) and next-to-nearest ($\langle ic_1c_{2L-1}\rangle$, dashed) neighbors, as well as the occupation of the site L ($\langle n_L\rangle$, dotted) during the adiabatic ramp.

For the "zig-zag" chain we can start with two decoupled closed chains (with even and odd lattice sites) when only Δ_2 and J_2 are nonzero but $\Delta_1 = J_1 = 0$. We then cut them as described above into two open chains each with two edge Majorana modes and in the even fermionic parity state with all fermions being paired. Now we can switch J_1 and Δ_1 on adiabatically to create a single quantum chain with even parity. Note that during this process there is no single-particle transition between the two subchains (with even and odd sites) because such a transfer would create single-particle excitations in both subchains which cannot occur in an adiabatic process due to the conservation of energy. Thus, each of the subchains remains in the even parity state.

Further increase of NN amplitudes results in a topological phase transition with closing the single-particle excitation gap allowing for a single-particle exchange between the subchains. Then, only the (even) parity of the entire chain is preserved.

Note that a similar idea can be used to create the initial Majorana state in the dissipative setting by adiabatically emptying one site [23].

TOF imaging

The calculation of the density distribution at the detector in a TOF experiment, $\langle n(x)\rangle = |\kappa|^2 \sum_{j,j'} e^{2ix(R_j - R_{j'})m/(\hbar t)} \langle a_j^\dagger a_{j'}\rangle$, where $|\kappa|^2 = 2mL/ht$, requires the knowledge of the first moments $\langle a_j^\dagger a_{j'}\rangle$ of the state in the lattice before the trapping potential is switched off. For the ideal Kitaev chain, the non-vanishing first moments in the Majorana language are $\langle c_{2j}c_{2k}\rangle_\pm = \langle c_{2j+1}c_{2k+1}\rangle_\pm = \delta_{kj}$, $\langle c_{2j}c_{2k+1}\rangle_\pm = -\langle c_{2j+1}c_{2k}\rangle_\pm = -i\delta_{kj}$, and the edge-edge correlations are given by $\langle c_{2L}c_1\rangle_\pm = im_\pm(d)$ [$m(d) = 0$ if we consider the bulk only] with d being the distance between the two Majorana edge modes. When only N_b sites on the right and on the left sides of the chain contribute to the signal (other sites are covered with a shade), the atom density distribution at the detector reads

$$\langle n(x)\rangle = |\kappa|^2 \Big\{ 2N_b \sin^2(\tfrac{mxa}{\hbar t}) + \Big[\cos(\tfrac{mxa}{\hbar t}) + \frac{1}{2} m(d) \cos(\tfrac{mxa}{\hbar t} d)\Big] \Big\}.$$

For the general case, we obtain the correlation matrix $\langle a_j^\dagger a_{j'}\rangle$ via a numerical diagonalization of the Hamiltonian H.

Spectroscopic detection of Majorana modes

We give the derivation of Eq. (2) for the ideal Kitaev chain. To this end we have to consider the effects of the perturbation $V(t) = (b_1^\dagger a_1 + b_L^\dagger a_L)e^{-i\Omega t} + h.c.$ on the Hamiltonian $H = H_K + \Delta E_b \sum_{j=1}^{M} b_j^\dagger b_j$, where $H_K = i2J_1 \sum_{l=1}^{L-1} c_{2l}c_{2l+1}$ is the ideal Kitaev chain Hamiltonian in the Majorana basis. Note that the Hamiltonian H_K is diagonal in the Bogoliubov quasiparticle basis $\tilde{a}_l = (a_l^\dagger - a_l + a_{l+1}^\dagger - a_{l+1})/2 = (c_{2l+1} + ic_{2l})/2$, $H_K = 2J_1 \sum_{l=1}^{L-1} \tilde{a}_l^\dagger \tilde{a}_l$, and its ground state is two-fold degenerate, with the ground states $|\Psi_+\rangle$ and $|\Psi_-\rangle$ having different fermionic parity.

We can now rewrite the external perturbation in terms of quasiparticle operators $\tilde{a}_l$ and Majorana operators γ_L, γ_R using $a_1 = (\gamma_L + \tilde{a}_1^\dagger - \tilde{a}_1)/2$, and $a_L = (\tilde{a}_{L-1}^\dagger + \tilde{a}_{L-1} - i\gamma_R)/2$. Choosing the even parity ground state $|\Psi_+\rangle$ as an initial state and using $\gamma_L|\Psi_\pm\rangle = |\Psi_\mp\rangle$ and $\gamma_R|\Psi_\pm\rangle = \pm i|\Psi_\mp\rangle$, a straightforward application of the standard time-dependent perturbation theory results in Eqs. (2) and (3) in the main text. If we go away from the ideal case, the ground state and the excitations can be determined numerically.